Time-resolved investigation of cobalt oxidation by Mn(III)-rich δ-MnO_2 using quick X-ray absorption spectroscopy

Anna A. Simanova[1], Jasquelin Peña[1*]

[1] Institute of Earth Surface Dynamics, University of Lausanne, Switzerland

[*] Corresponding author. E-mail: jasquelin.pena@unil.ch; Tel: +47216924355; 4879 Geopolis, UNIL-Mouline, CH-1015 Lausanne

SUPPORTING INFORMATION

(16 pages, 7 figures, 5 tables)

SI Materials and methods.

Pair distribution function analysis of high-energy X-ray scattering. Pair distribution function (PDF) analysis was used to determine whether any changes in mineral structure were caused by the adsorption of Co^{2+} and incorporation of Co^{3+} into the Mn^{III}_δ-MnO_2 structure. Samples analyzed by PDF analysis were equilibrated for 48 hours and thus reflect structural changes incurred over longer reaction times than those investigated by QXAS (t < 12 h). The PDFs were extracted from high-energy X-ray scattering data collected using X-rays of 58.65 keV (λ = 0.2114 Å) on beam line 11-ID-B at the Advanced Photon Source, Argonne National Laboratory. Data were collected to Q values of 29 $Å^{-1}$ at room temperature. The solids from 20 mL of a Mn^{III}_δ-MnO_2 suspension equilibrated with Co to achieve maximum surface loadings of 0, 0.05, or 0.20 mol Co mol^{-1} Mn (**Table S1**) were obtained by filtration, air-dried overnight and packed into Kapton capillaries (inner diameter of 1 mm, Cole-Parmer); the capillaries were sealed on both ends using epoxy.

In the program Fit2D,[1] the 2D scattering patterns were first corrected for sample-to-detector distance and tilt angle of the detector relative to the beam path, then integrated and converted to 1D plots of the scattering intensity versus scattering angle, Q. In the program PDFgetX2,[2] the 1D plots were converted to the total structure function, S(Q), and the PDF, G(R), using standard correction and normalization procedures.[3] The chemical formulas used for data reduction were $Na_{0.03}MnO_2{\cdot}xH_2O$, $Co_{0.04}Na_{0.03}MnO_2{\cdot}xH_2O$, $Co_{0.21}Na_{0.03}MnO_2{\cdot}xH_2O$ for Co_0.00, Co_0.05 and Co_0.20, respectively, where Na:Mn and Co:Mn molar ratios were obtained from chemical analysis of the solid by ICP-OES and the number of water molecules (*x*) was varied

between 2 and 3 to minimize variations in the background signal between 0 – 1.5 $Å^{-1}$. Differential PDFs (d-PDFs) were obtained by subtracting the PDF of Co_0.00 from Co_0.05 and Co_0.20 samples to identify changes in mineral structure induced by Co sorption.[4-6]

Effect of HEPES on Co uptake and Mn(II) release in Co-Mn^{III}_δ-MnO_2

Due to the presence of a reducing piperazine-ring group, HEPES may interfere with Co-Mn redox processes by 1) generating additional Mn(III) by reducing Mn(IV), 2) generating Mn(II) by reducing Mn(III) or 3) sorbing and thus blocking reactive surface sites. To test the effect of the HEPES buffer on Co uptake and Mn release to solution, we performed complementary experiments where, prior to Co addition, the Mn^{III}_δ-MnO_2 particles were filtered to remove all HEPES, rinsed with 10 mM NaCl and resuspended in 10 mM NaCl. In these experiments, a pH STAT (Metrohm) was used for pH-control. After 1-hour equilibration at pH 6.5, an aliquot of $CoCl_2$ solution was added to achieve a total Co concentration of 0.20 mol Co mol^{-1} Mn. Samples were withdrawn as a function of time to analyze for the total and aqueous concentrations of Co and Mn. In addition, we measured AMON values (potentiometric titrations) and Mn(III) content (pyrophosphate extractions) in the HEPES-reacted δ-MnO_2 as a function of time in the absence of Co.

In the absence of Co, we found that the Mn(III) content of the Mn oxide reached 31 % within 1 h of the reaction of δ-MnO_2 with HEPES and increased only slightly (to 35 %) from 1 h to 48 h. By 48 h of the reaction, around 1 % of the Mn initially in the solid was accumulated in solution as Mn(II). Our previous study showed that equilibration of δ-MnO_2 with HEPES under these experimental conditions does not trigger any phase

transformation.[7] These observations suggest that HEPES has a diminished effect on Mn(III) generation as the mineral approaches the maximum amount of Mn(III) it can accommodate.[8]

Our experiments in the presence of Co showed no difference in Co uptake and Mn release kinetics at t < 100 min in the presence and absence of HEPES (Figure S3), but slightly greater Mn release in the presence of HEPES at t > 100 min (8 % vs. 5 %). Since the extent of Co sorption by Mn^{III}_δ-MnO_2 is the same in the presence and absence of HEPES, we do not expect significant amounts of HEPES to accumulate at the surface and compete with Co for the same surface sites. Unmodified kinetics and extent of Co uptake even with an initial 10-fold excess of HEPES also indicates that cobalt must have a significantly greater affinity/reactivity towards the mineral. In addition, the similarity in the kinetics and extent of Mn(II) accumulation in solution with and without HEPES during first 100 min corroborates that aqueous Mn(II) originates from sorption/redox reactions between Co and the mineral. This conclusion is also consistent with the fact that the addition of Co triggers 5-8 % of the total Mn initially in the solid phase accumulated in solution as Mn(II), compared to about 1 % Mn released in the absence of Co after 48 h of reaction with HEPES.[7] However, from 100 min to 48 h, slightly more Mn(II) was released in Co-Mn^{III}_δ-MnO_2 experiments the presence of HEPES (8 % at 48 h) than in its absence (5% at 48 h).

Assuming that significant changes in the mechanism of Co sorption and oxidation by Mn(III)_δ-MnO_2 would lead to different reaction kinetics, we conclude that HEPES does not influence the Co uptake mechanism at t < 100 min, but may have a small influence at t > 100 min. Slightly higher Mn release at t > 100 min may be consistent

with i) HEPES consumption of Mn(III); ii) disproportionation of Mn(III) atoms, where Mn(III) could originate from Co or HEPES oxidation coupled to Mn(IV) reduction; 3) slow desorption of adsorbed Mn(II), where Mn(II) could originate from Co or HEPES oxidation coupled to Mn(III) reduction. Due to the plethora of processes, we cannot ascertain whether the slight increase in Mn release at reaction times greater than 100 min is due to redox processes involving Co, HEPES or both Co and HEPES.

SI Figures

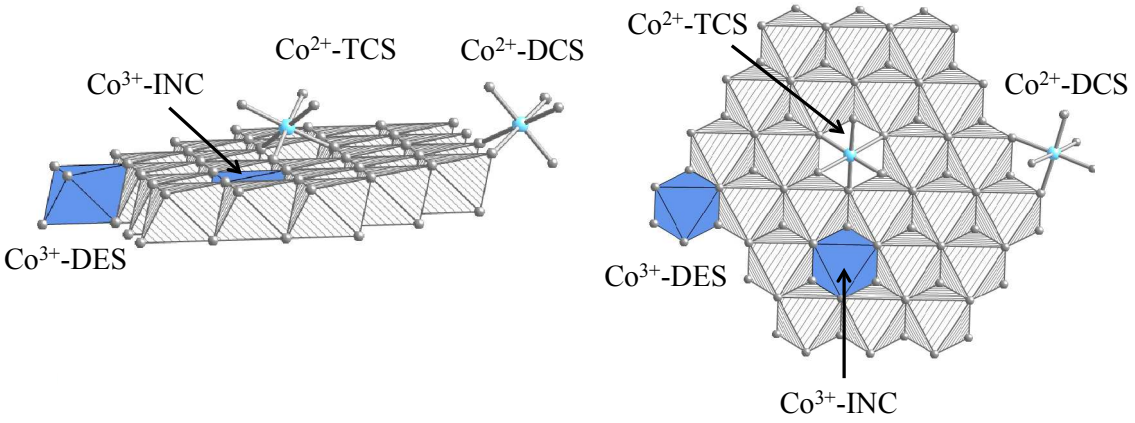

Figure S1. Schematic representations of Co-MnO_2 surface complexes (left - side view, right – top view): Co^{2+} = light blue, Co^{3+} = dark blue, Mn octahedra = hatched, O = grey.

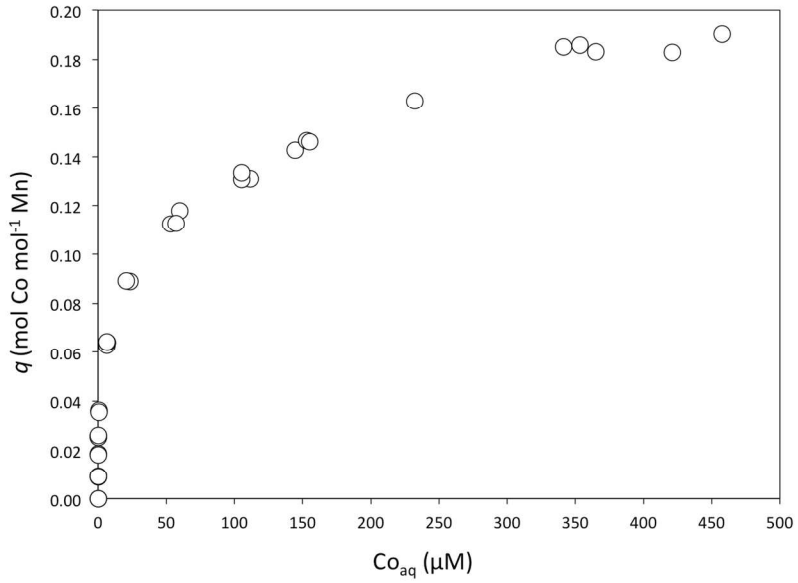

Figure S2. Sorption isotherm of Co on Mn^{III}_δ-MnO_2 measured at pH 6.5 after 48 h of equilibration following the experimental procedure described in the main manuscript text.

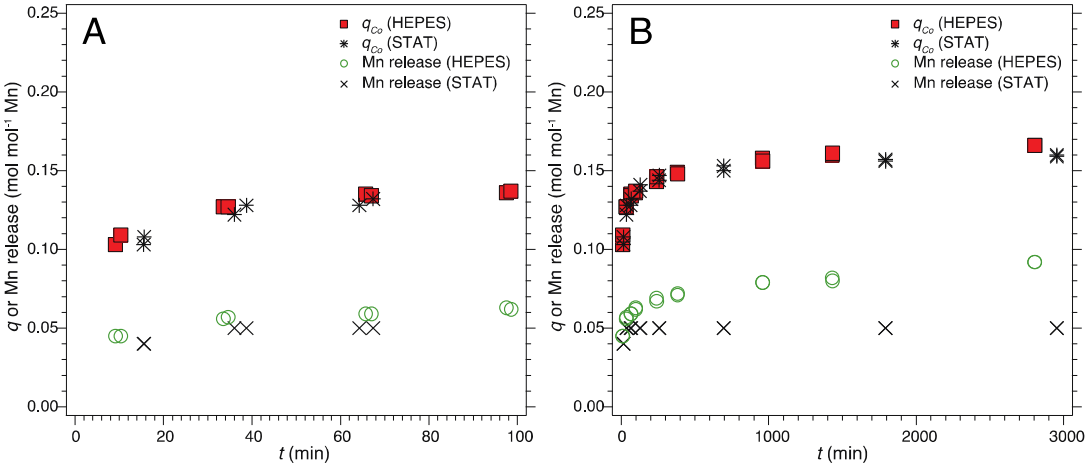

Figure S3. Batch kinetic data obtained for Co sorption and Mn release in Mn^{III}_δ-MnO_2 suspension at total Co concentration of 0.20 mol Co mol^{-1} Mn at pH 6.5 in the presence and absence of 10 mM HEPES (pH maintained with STAT) during first 100 min (A) and during 3000 min (B).

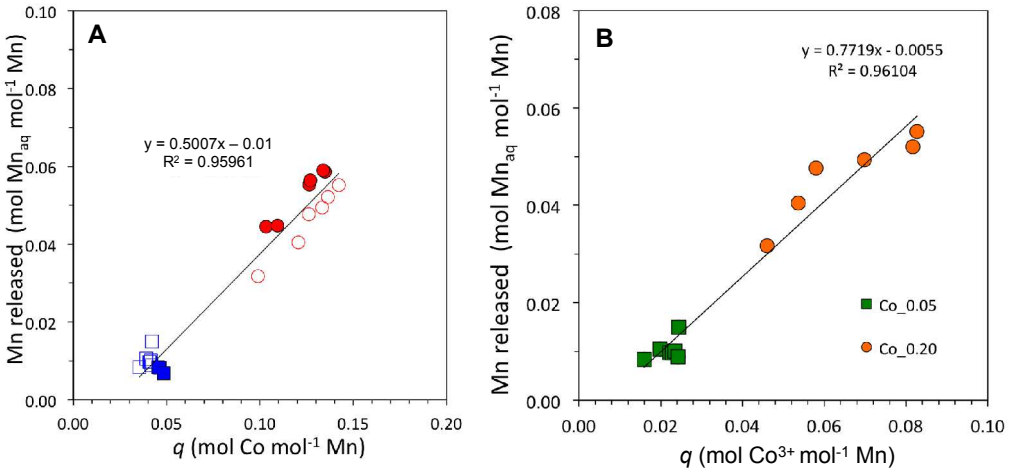

Figure S4. (A) Plot of Mn released against Co surface excess (q) measured in batch kinetic (filled symbols) and QXAS (empty symbols) experiments in Co_0.05 (squares) and Co_0.20 (circles) experiments at t < 30 min. (B) Plot of Mn released against Co^{3+} surface excess in Co_0.05 and Co_0.20 experiments at t < 30 min.

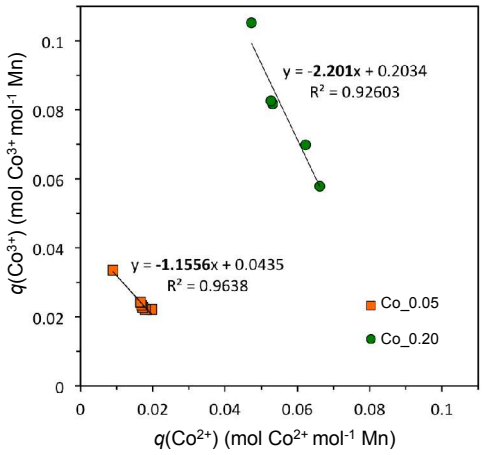

Figure S5. Plots of the Co^{3+} surface excess against the Co^{2+} surface excess in Co_0.05 and Co_0.20 at reaction times between 20 min and 12 h. The linear correlations show that in Co 0.05 $\Delta q(Co^{3+})/\Delta q(Co^{2+})$ is close to -1, while in Co 0.20 $\Delta q(Co^{3+})/\Delta q(Co^{2+})$ is close to -2.

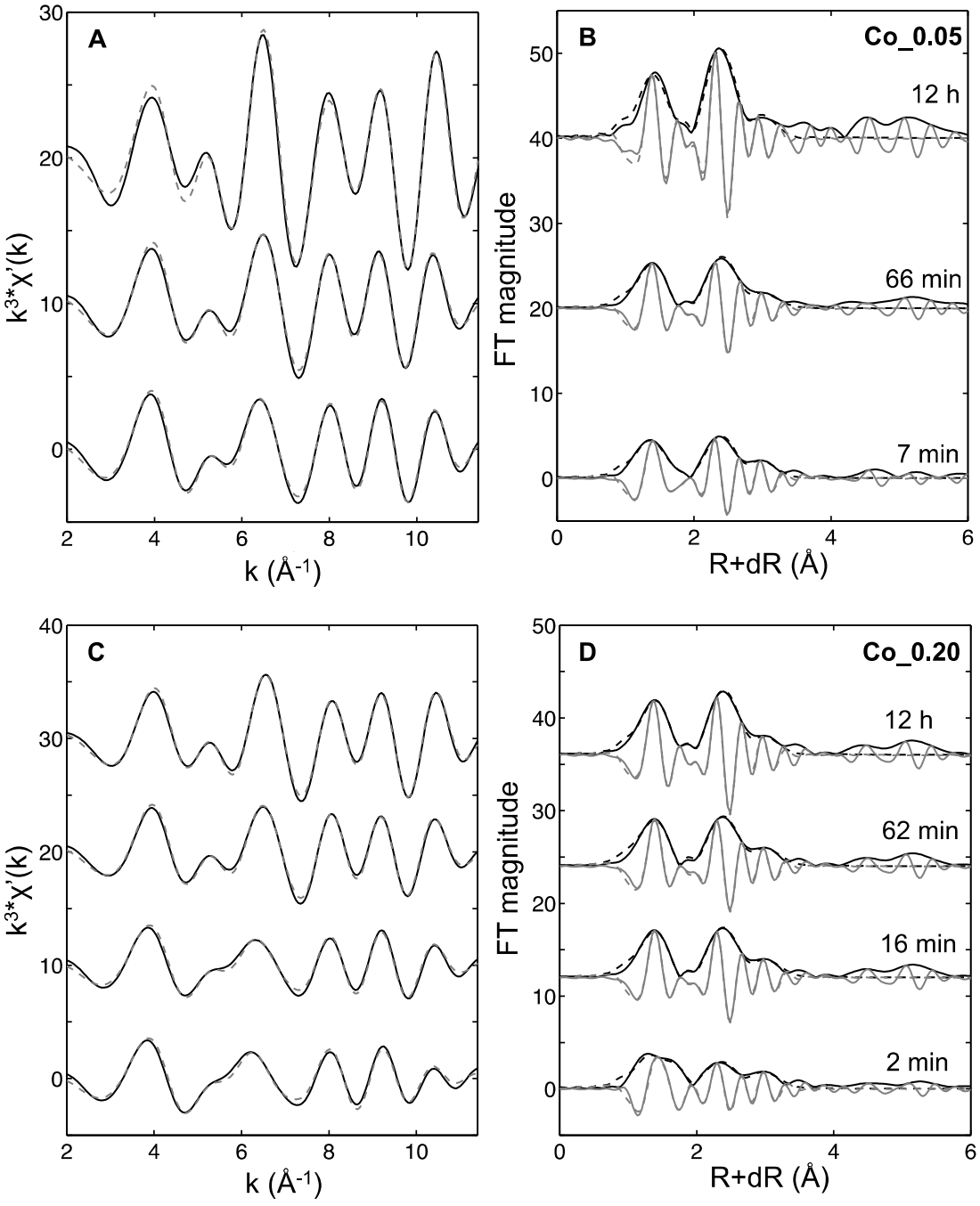

166

167 **Figure S6**. Back Fourier-transforms taken from 1-3.3 Å (left) and magnitude and
168 imaginary parts of the Fourier-transforms (right) of the Co K-edge EXAFS spectra for
169 Co_0.05 (A and B) and Co_0.20 (C and D) plotted with best-fit curves (dashed lines)
170

171

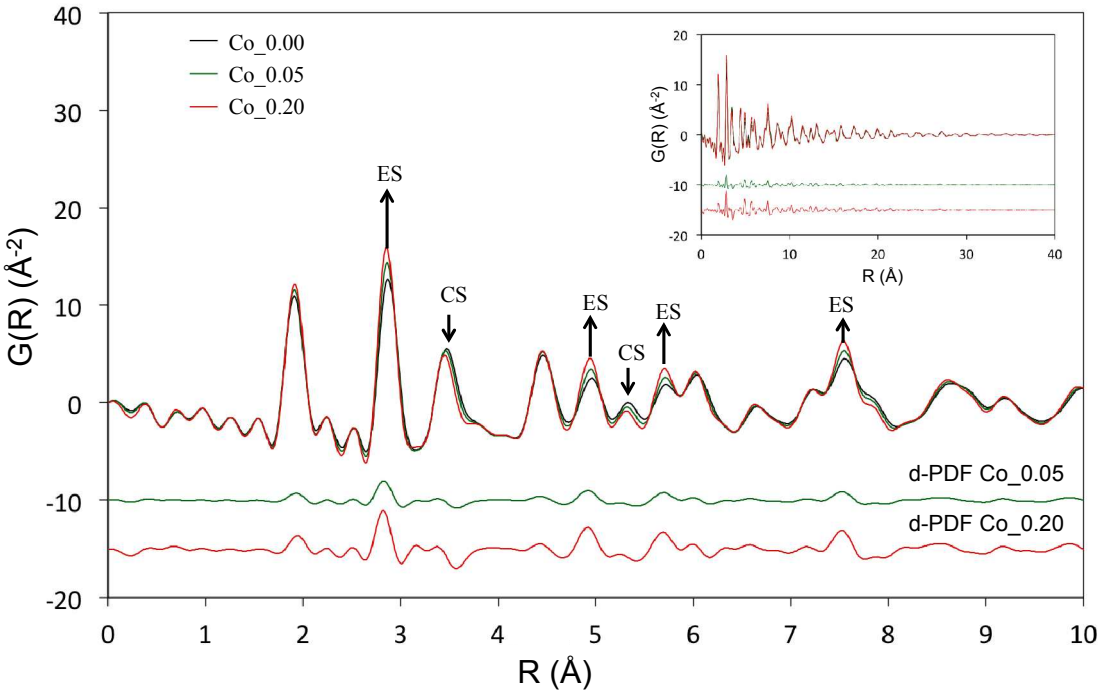

Figure S7. PDFs Co_0.00, Co_0.05, and C0_0.20. The arrows indicate differences in the spectra observed as a function of the Co loading. Peaks were assigned based on the work by Manceau et al.[8]; "CS" denotes corner-sharing linkages between Me(layer)–Me(interlayer) pairs, "ES" denotes edge-sharing linkages between Me(layer)–Me(layer) pairs. Differential PDFs obtained by subtracting the PDF of Co_0.00 from the PDFs of Co_0.05 and Co_0.20 are shown at the bottom of the figure. The inset shows the PDFs extended to up to 40 Å.

Table S1. Description of samples obtained from batch kinetic, QXAS and PDF measurements.

	time	pH	c_{MnTOT}, µM	c_{CoTOT}, µM	c_{Mn}, µM[a]	c_{Co}, µM	q_{max}[b]	q[c]	Mn release[d]
Batch kinetic									
Co_0.00	10 min	6.68	4474.97	-	1.2	-	-	-	0.000
	48 h				58.67				0.013
Co_0.05	10 min	6.69	4578.46	235.4	37.8	26.06	0.05	0.05	0.008
	48 h				121.84	1.35	0.05	0.05	0.027
Co_0.20	10 min	6.35	5121.48	1008.53	228.01	473.02	0.20	0.11	0.045
	48 h				471.18	235.91	0.20	0.17	0.092
QXAS samples									
Co_0.05	12 h	6.74	8501.80	365.27	127.36	13.70	0.04	0.04	0.02
Co_0.20	12 h	6.67	6914.93	1257.93	402.74	260.17	0.18	0.15	0.06
PDF samples									
Co_0.00	48 h	6.81	7495.03	-	64.92	-	-	-	0.01
Co_0.05	48 h	6.34	6601.47	268.13	131.20	1.38	0.04	0.04	0.02
Co_0.20	48 h	6.30	6602.00	1519.13	505.43	224.35	0.23	0.21	0.08

[a] the concentrations of aqueous Mn in Co 0.05 and Co 0.20 are not corrected to the concentrations of aqueous Mn in the blank experiment (Co 0.00)
[b] q_{max} is the theoretical maximum surface loading of Co that was calculated as c_{CoTOT}/c_{MnTOT}
[c] q is the amount of Co sorbed per mol Mn and was calculated as $(c_{CoTOT} - c_{Co})/(c_{MnTOT} - c_{Mn})$
[d] Mn release was calculated as c_{Mnaq}/c_{MnTOT} ad has units of mol Mn_{aq} mol^{-1} Mn. Note that values for the Mn release in Co 0.05 and Co 0.20 are not corrected to the values of the Mn release in the blank experiment (Co 0.00)

207 **Table S2.** LCF results, where *f* is the fraction of Co^{2+} and (1-*f*) is the fraction of Co^{3+}.

	t, min	*q*	*f*	*1-f*	Comp Sum	*q* (Co^{2+})	*q* (Co^{3+})
Co_0.05[a]	2	0.035	0.53[b]	0.45[b]	0.98	0.019	0.016
	7	0.039	0.47	0.51	0.98	0.018	0.020
	15	0.043	0.46	0.52	0.98	0.020	0.022
	21	0.041	0.44	0.54	0.98	0.018	0.022
	28	0.041	0.42	0.56	0.98	0.017	0.023
	36	0.042	0.41	0.57	0.98	0.017	0.024
	49	0.042	0.40	0.58	0.98	0.017	0.024
	66	0.042	0.40	0.58	0.98	0.017	0.024
	720	0.043	0.21	0.80	1.01	0.009	0.034
Co_0.20[a]	2	0.099	0.53	0.46	0.99	0.052	0.046
	8	0.121	0.54	0.45	0.99	0.065	0.054
	16	0.126	0.52	0.46	0.98	0.066	0.058
	25	0.133	0.47	0.52	0.99	0.063	0.069
	35	0.136	0.39	0.60	0.99	0.053	0.082
	62	0.142	0.37	0.58	0.95	0.053	0.082
	720	0.153	0.31	0.69	1.00	0.047	0.106

208 [a] For all samples the reduced chi^2 values ranged 0.0003 – 0.0024
209 [b] Uncertainties for *f* for all samples were in a range 0.002 – 0.005

Table S3. Structural parameters for Co_0.05 on Mn^{III}_δ-MnO_2.

Sample	Shell ID	A[a]	R, Å	σ^2, Å^2	ΔE_0, eV	Red χ^2	R-factor	CN(Co^{3+}-Mn^{ES})	CN(Co^{2+}-Mn^{CS})
Co_0.05	Co^{3+}-O	6·(1-f)	1.91±0.01	0.0050±0.0010	-9.7±1.1	0.00	0.0157		
7 min	Co^{2+}-O	6·f	2.08±0.01	0.0052±0.0014					
	Co^{3+}-Mn^{ES}	CN(Co^{3+}-M^{ES})·(1-f)	2.84±0.01	0.0025±0.0010				3.12±0.49	
	Co^{2+}-Mn^{CS}	CN(Co^{2+}-Mn^{CS})·f	3.48±0.01	0.004[b]					2.71±0.43
Co_0.05	Co^{3+}-O	6·(1-f)	1.92±0.01	0.0049±0.0009	-8.7±1.0	0.02	0.0132		
66 min	Co^{2+}-O	6·f	2.10±0.02	0.0081±0.0025					
	Co^{3+}-Mn^{ES}	CN(Co^{3+}-M^{ES})·(1-f)	2.85±0.01	0.0035±0.0010				3.84±0.52	
	Co^{2+}-Mn^{CS}	CN(Co^{2+}-Mn^{CS})·f	3.50±0.01	0.004					2.90±0.55
Co 0.05	Co^{3+}-O	6·(1-f)	1.91±0.01	0.0037±0.0008	-11.5±1.4	20.41	0.0203		
12 h	Co^{2+}-O	6·f	2.12±0.03	0.0040±0.0041					
	Co^{3+}-Mn^{ES}	CN(Co^{3+}-M^{ES})·(1-f)	2.84±0.01	0.0022±0.0009				4.13±0.62	
	Co^{2+}-Mn^{CS}	CN(Co^{2+}-Mn^{CS})·f	3.43±0.02	0.004					5.39±1.76
		Nind/Nvar	19/10						

[a] A denotes the amplitude of the corresponding shell, which equals the coordination number (CN) scaled by the fraction of Co^{2+} (f) and Co^{3+} (1-f) that was obtained by LCF fitting of the QXANES spectra (**Table S2**). The coordination numbers of Co-O shells were fixed to 6, while the coordination numbers of Co-Mn shells [CN(Co^{3+}-Mn^{ES}) and CN(Co^{2+}-Mn^{CS})] were floated

[b] The Debye-Waller factor was fixed to the value reported previously.[9]

Table S4. Structural parameters for Co_0.20 on Mn^{III}_δ-MnO_2.

Sample	Shell ID	A[a]	R, Å	σ^2, Å^2	ΔE_0, eV	Red χ^2	R-factor	CN(Co^{3+}-Mn^{ES})	CN(Co^{2+}-Mn^{CS})
Co_0.20	Co^{3+}-O	6·(1-f)	1.91±0.01	0.0075±0.0018	-10.9±1.6	0.11	0.0367		
2 min	Co^{2+}-O	6·f	2.08±0.01	0.0041±0.0012					
	Co^{3+}-Mn^{ES}	CN(Co^{3+}-M^{ES})·(1-f)	2.83±0.01	0.0033±0.0021				2.37±0.75	
	Co^{2+}-Mn^{CS}	CN(Co^{2+}-Mn^{CS})·f	3.48±0.02	0.004[b]					2.21±0.47
Co_0.20	Co^{3+}-O	6·(1-f)	1.91±0.01	0.0052±0.0011	-9.9±1.4	0.05	0.0279		
16 min	Co^{2+}-O	6·f	2.09±0.01	0.0054±0.0013					
	Co^{3+}-Mn^{ES}	CN(Co^{3+}-Mn^{ES})·(1-f)	2.84±0.01	0.0020±0.0015				2.34±0.55	
	Co^{2+}-Mn^{CS}	CN(Co^{2+}-Mn^{CS})·f	3.49±0.01	0.004					2.14±0.42
Co_0.20	Co^{3+}-O	6·(1-f)	1.92±0.01	0.0053±0.0008	-9.2±0.9	0.06	0.0117		
62 min	Co^{2+}-O	6·f	2.10±0.01	0.0070±0.0019					
	Co^{3+}-Mn^{ES}	CN(Co^{3+}-Mn^{ES})·(1-f)	2.84±0.01	0.0040±0.0009				3.57±0.47	
	Co^{2+}-Mn^{CS}	CN(Co^{2+}-Mn^{CS})·f	3.49±0.01	0.004					3.25±0.48
Co_0.20	Co^{3+}-O	6·(1-f)	1.91±0.01	0.0048±0.0006	-8.8±0.8	2.44	0.0088		
12 h	Co^{2+}-O	6·f	2.11±0.02	0.0072±0.0022					
	Co^{3+}-Mn^{ES}	CN(Co^{3+}-Mn^{ES})·(1-f)	2.83±0.01	0.0032±0.0007				3.70±0.41	
	Co^{2+}-Mn^{CS}	CN(Co^{2+}-Mn^{CS})·f	3.47±0.01	0.004					3.73±0.59
	Nind/Nvar	19/10							

[a] A denotes the amplitude of the corresponding shell, which equals the coordination number (CN) scaled by the fraction of Co^{2+} (f) and Co^{3+} (1-f) that was obtained by LCF fitting of the QXANES spectra (**Table S2**). The coordination numbers of Co-O shells were fixed to 6, while the coordination numbers of Co-Mn shells [CN(Co^{3+}-Mn^{ES}) and CN(Co^{2+}-Mn^{CS})] were floated

[b] The Debye-Waller factor was fixed to the value reported previously.[9]

Table S5. Changes in Co^{2+} and Co^{3+} surface speciation at the surface of Mn^{III}_δ-MnO_2 as a function of time in Co_0.05 and Co_0.20.

	t, min	q (Co^{2+}-DCS)[a]	q ($Co^{2,3+}$-TCS)	error[b] in q($Co^{2,3+}$-CS)	q (Co^{3+}-DES)	q (Co^{3+}-INC)	error in q(Co^{3+}-ES)
Co_0.05	7	0.015	0.003	±0.002	0.014	0.006	±0.002
	66	0.013	0.004	±0.002	0.013	0.011	±0.003
	720	nd	0.008	±0.004	0.016	0.018	±0.005
Co_0.20	2	0.052	nd	±0.003	0.042	nd	±0.009
	16	0.066	nd	±0.005	0.053	nd	±0.008
	62	0.037	0.017	±0.006	0.050	0.032	±0.010
	720	0.027	0.020	±0.007	0.061	0.045	±0.011

[a] Surface excess of the various Co surface species estimated as the product of the Co surface loading (q), the fractions of Co^{2+} and Co^{3+} obtained from the LCF-QXANES (**Table S2**) and the *CN*s of the corresponding Co-Mn shells obtained from shell-by-shell fitting to the QEXAFS spectra (**Tables S3** and **S4**)

[b] Uncertainty in the surface excesses of the CS and ES geometries were estimated based on the uncertainty in the *CN*s of the corresponding Co-Mn shells (**Tables S3** and **S4**)

[c] nd = not detected, i.e. the estimated surface excess was lower than the uncertainty

References

(1) Hammersley, A. P.; Svensson, S. O.; Hanfland, M.; Fitch, A. N.; Hausermann, D., Two-dimensional detector software: From real detector to idealised image or two-theta scan. *High Pressure Research* **1996,** *14*, (4-6), 235-248.

(2) Farrow, C. L.; Juhas, P.; Liu, J. W.; Bryndin, D.; Bozin, E. S.; Bloch, J.; Proffen, T.; Billinge, S. J. L., PDFfit2 and PDFgui: computer programs for studying nanostructure in crystals. *Journal of Physics-Condensed Matter* **2007,** *19*, (33), 335219.

(3) Chupas, P. J.; Qiu, X.; Hanson, J. C.; Lee, P. L.; Grey, C. P.; Billinge, S. J. L., Rapid-acquisition pair distribution function (RA-PDF) analysis. *Journal of Applied Crystallography* **2003,** *36*, (6), 1342-1347.

(4) Harrington, R.; Hausner, D. B.; Bhandari, N.; Strongin, D. R.; Chapman, K. W.; Chupas, P. J.; Middlemiss, D. S.; Grey, C. P.; Parise, J. B., Investigation of surface structures by powder diffraction: a differential pair distribution Function study on arsenate sorption on ferrihydrite. *Inorg. Chem.* **2010,** *49*, (1), 325-330.

(5) Li, W.; Harrington, R.; Tang, Y. Z.; Kubicki, J. D.; Aryanpour, M.; Reeder, R. J.; Parise, J. B.; Phillips, B. L., Differential pair distribution function study of the structure of arsenate adsorbed on nanocrystalline gamma-alumina. *Environ. Sci. Technol.* **2011,** *45*, (22), 9687-9692.

(6) Wang, X. M.; Li, W.; Harrington, R.; Liu, F.; Parise, J. B.; Feng, X. H.; Sparks, D. L., Effect of ferrihydrite crystallite size on phosphate adsorption reactivity. *Environ. Sci. Technol.* **2013,** *47*, (18), 10322-10331.

(7) Simanova, A. A.; Kwon, K. D.; Bone, S. E.; Bargar, J. R.; Refson, K.; Sposito, G.; Peña, J., Probing the sorption reactivity of the edge surfaces in birnessite nanoparticles using nickel(II). *Geochim. Cosmochim. Acta* **2015,** *164*, (0), 191-204.
(8) Manceau, A.; Marcus, M. A.; Grangeon, S.; Lanson, M.; Lanson, B.; Gaillot, A. C.; Skanthakumar, S.; Soderholm, L., Short-range and long-range order of phyllomanganate nanoparticles determined using high-energy X-ray scattering. *Journal of Applied Crystallography* **2013,** *46*, (1), 193-209.
(9) Manceau, A.; Drits, V. A.; Silvester, E.; Bartoli, C.; Lanson, B., Structural mechanism of Co^{2+} oxidation by the phyllomanganate buserite. *Am. Mineral.* **1997,** *82*, (11-12), 1150-1175.